GEOPHYSICAL RESEARCH LETTERS, VOL. 27, NO. 21, PAGES 3449-3452, NOVEMBER 1, 2000

Ozone profiles from 30 to 110 km measured by the Occultation RAdiometer instrument during the period Aug 1992-Apr 1993.

Didier Fussen, Filip Vanhellemont, Christine Bingen
and Simon Chabrillat
Institut d'Aéronomie Spatiale de Belgique, Brussels

Abstract. We present ozone volume mixing ratio profiles obtained by the ORA instrument during the period Aug 1992-Apr 1993. They have been retrieved by applying a specific inversion algorithm to a radiometric UV channel contaminated by Rayleigh scattering. The results compare reasonably well with other instruments up to the mesopause and are probably the first extended ozone data in the lower thermosphere (90-110 km).

1. Introduction

The Occultation RAdiometer (ORA), a simple UV-visible instrument for atmospheric remote sensing by the solar occultation method, has been developed by the Belgian Institute for Space Aeronomy. It was launched in July 1992 on board the EUropean REtrievable CArrier for a one year mission. The instrument was dedicated to the measurement of stratospheric vertical profiles of O_3, NO_2, H_2O number densities as well as the extinction coefficient of aerosols by using 8 broadband channels ranging from 260 nm to 1013 nm.

ORA recorded about 7000 orbital sunsets and sunrises through the Earth's atmosphere from an altitude of about 500 km. The geolocations of the tangent points lie between 40° S and 40° N due to the low-orbit inclination (28°). In previous publications [*Fussen et al.*, 1997, 1998], we presented the results obtained by the application of a dedicated inversion method. Indeed, the instrument has a large field of view (±2°) suggesting a *apparent* coarse vertical resolution ($\simeq 20\,km$) determined by the Sun's angular size itself. However, this fact is balanced by the quality of the transmittance signal that has a very large signal-to-noise ratio only limited by the digitization (16 bits).

A specific channel was devoted to the study of mesospheric ozone profiles by using the important absorption near the maximum of the Hartley band (260 nm). Unfortunately, this channel was known to be defective before the flight due to a small parasitic transmission window at about 340 nm enhanced by the stronger solar irradiance in that domain. Indeed, the observed transmittance signal turned out to be strongly structured, reflecting the competition between ozone absorption and Rayleigh scattering.

We present the specific retrieving algorithm for this channel and a first analysis of the obtained ozone fields from the stratosphere up to the lower thermosphere.

Copyright 2000 by the American Geophysical Union.

Paper number 2000GL011575.
0094-8276/00/2000GL011575$05.00

2. Inversion algorithm

A schematic view of the occultation geometry is presented in Fig. 1. The mean tangent altitude h_0 is defined by the straight line joining the satellite and the center of the Sun, assuming that refraction may be neglected above $h_0 \simeq 30\ km$. The Earth's radius R is determined by the sphere tangent to the geoid. The detector records the light emitted by the whole solar disk having an angular size of about 9.3 mrad. This corresponds to a vertical domain of 22 km for the observed atmospheric region at $h_0 = 80\ km$.

The transmittance , defined as the ratio of the occultation signal to the signal measured outside the atmosphere, may be written as

$$T(h_0) = \int_{\lambda_1}^{\lambda_2} \int_{\alpha_1}^{\alpha_2} F(\lambda) G(\alpha, \lambda) \exp(-\tau(\alpha, \lambda))\, d\alpha\, d\lambda \quad (1)$$

where the integral over λ covers the nominal spectral range in the Hartley band as well as the parasite spectral window up to 360 nm. The filter function $F(\lambda)$ contains all the spectral information related with the nominal filter transmittance, the detector sensitivity and the solar irradiance. A second integration runs over the angular domain $[\alpha_1, \alpha_2]$ defining the apparent Sun that is discretized into horizontal slices (a number of 10 slices was found to be a good trade-off between computing time and accuracy). Each slice observed under an angle α can be associated to a tangent height $h(\alpha)$ given by

$$h(\alpha) = \frac{\sqrt{R_\odot^2 - (h_0 + R)^2} + (h_0 + R)}{\sqrt{1 + \tan(\alpha)^2}} - R \quad (2)$$

The contribution of each slice is weighted by an intensity distribution function $G(\alpha, \lambda)$ across the solar disk that takes into account the relative surface of the slice and the solar limb darkening function [*Allen*, 1985]. According to Bouguer's law, all rays emitted from a particular slice are exponentially attenuated with respect to the slant path optical thickness $\tau(\alpha, \lambda)$ obtained as a third integration along the optical path of the total extinction coefficient $\beta(z, \lambda)$:

$$\tau(\alpha, \lambda) = \int_{s_1}^{s_2} \beta(z(s), \lambda)\, ds \quad (3)$$

The s_1 and s_2 values define the entrance and exit points in the Earth's atmosphere and the local altitude z is related to the optical path length element s by

$$z = \sqrt{s^2 + (h(\alpha) + R)^2} - R \quad (4)$$

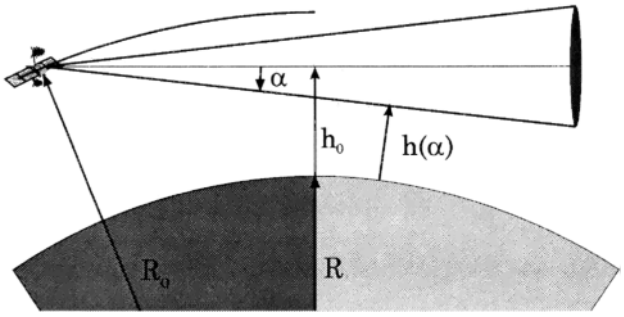

Figure 1. Geometry of a solar occultation

Although a very accurate knowledge of $F(\lambda)$ is usually not critical in an occultation experiment where a monochromatic transmittance is measured (with respect to the intensity recorded outside the atmosphere), this was not the case here where both Rayleigh scattering and ozone absorption may interfere (see Fig. 2).

Some tentatives to re-construct $F(\lambda)$ from pre-flight or post-flight instrument characteristics and published solar irradiance values [*Kurucz et al.*, 1984] were not satisfactory mainly because the temporal evolution of photodiode characteristics was not accurately known. Furthermore, the degradation of the optics was not a linear function of the mission elapsed time. Therefore, we decided to adopt a heuristic procedure where we modelized $F(\lambda)$ as a bi-gaussian function

$$F(\lambda) = c_1 \exp(-(\frac{\lambda - c_2}{c_3})^2) + c_4 \exp(-(\frac{\lambda - c_5}{c_6})^2) \quad (5)$$

From inspection of the signal, it is clear that the major interference between air and ozone takes place in the $[30 - 70\ km]$ altitude range. For each ORA mission elapsed day, we used US76 [*National Oceanic and Atmospheric Organization*, 1976] standard atmospheric air and ozone profiles to generate a synthetic transmittance. In this low altitude subrange, a non-linear optimization of the set of c_i $\{i = 1..6\}$ was then performed to obtain an accurate fit of one measured event for each day. The ratio of ozone and air cross sections is not the same at different wavelengths and this allows the algorithm to converge toward a solution with well separated centroids. This procedure gives the most probable filter function with respect to a mean atmosphere and it is expected that the temporal evolution of the filter characteristics is smooth, continuous and does not reflect deviations of true ozone profiles with respect to mean values. In the $[30 - 70\ km]$ altitude range, the filter function optimization is strongly constrained to reproduce both ozone and air contributions in both spectral regions. It should be noted that this empirical determination of $F(\lambda)$ remains independent of the transmittance measured between 70 and 120 km.

The retrieved centroids (c_2 = 272.5±2.4 nm and c_5 = 342.4±4.3 nm) and widths ($c_3 \simeq c_6 \simeq 5$ nm) turned out to be very stable during the mission (indicating the absence of wavelength shift) and we present the evolution of $c_{1,2}$ and $c_{4,5}$ in Fig. 3. All coefficients have a well correlated temporal evolution which cannot be attributed to a progressive deviation of ozone with respect to the climatology. Latitudinal effects appear also to be negligible. The relative importance of the nominal filter and of the leak (represented by c_1 and c_4, respectively) showed clearly a strong degradation of the former during the mission. This is probably caused by some opacification of the radiometer optics due to intense UV radiation.

Assuming that the time evolution of the $c_i(t)$ is valid for all events of the same day, the forward model is fully defined by renormalizing $F(\lambda)$ and $G(\alpha, \lambda)$ by

$$\int_{\lambda_1}^{\lambda_2} \int_{\alpha_1}^{\alpha_2} F(\lambda) G(\alpha, \lambda)\, d\alpha\, d\lambda = 1 \quad (6)$$

The total extinction coefficient $\beta(z, \lambda)$ can be expressed as a sum of products of absorption cross sections times the associated number density profiles as

$$\beta(z, \lambda) = \sigma_{O_3}(\lambda)\, n_{O_3}(z) + \sigma_{Rayleigh}(\lambda)\, n_{Air}(z) \quad (7)$$

The temperature dependence of the ozone cross section [*Burrows et al.*, 1999] in the Huggins band has been considered. An equivalent cross section was computed by integrating the temperature dependent cross section over the optical path and by using climatological temperature profiles.

The large angular field of view of ORA is responsible for an important overlap between two successive measurements along the orbit, which may cause severe ill-conditioning in the inversion of $T(h_0)$. Therefore we preferred to develop the unknown density profiles on a basis of Chebyshev orthogonal polynomials $P_i(z)$ (defined in the range $[0 - 150\ km]$):

$$n_{O_3}(z) = \widetilde{n}_{O_3}(z) \sum_{i=0}^{N_{O_3}} a_i^{O_3} P_i(z) \quad (8)$$

$$n_{Air}(z) = \widetilde{n}_{Air}(z) \sum_{i=0}^{N_{Air}} a_i^{Air} P_i(z) \quad (9)$$

where $a_i^{O_3}$, a_i^{Air} are unknown coefficients defining the relative ozone and air number density profiles ($\widetilde{n}_{O_3}(z)$, $\widetilde{n}_{Air}(z)$ are standard atmospheric profiles used for a correct scaling of the problem). The inversion problem can now be solved

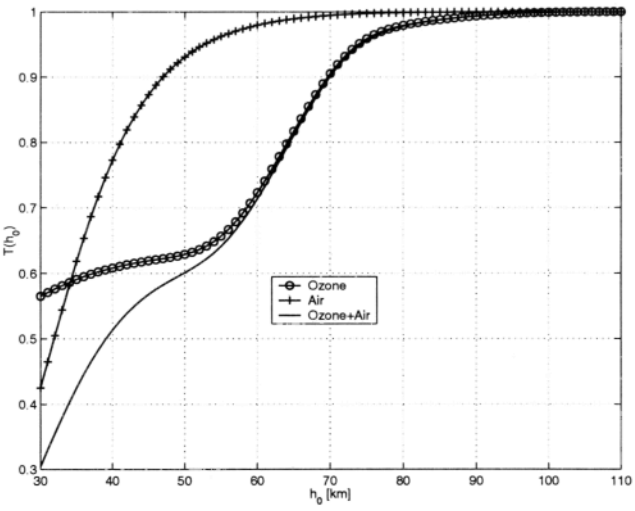

Figure 2. Observed total transmittance signal (full line) and best fit calculated contributions for ozone (circles) and air (crosses)

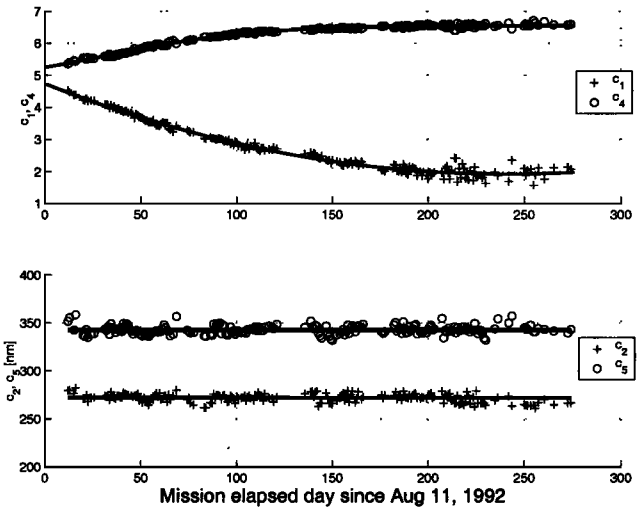

Figure 3. Temporal evolution of the filter coefficients c_1 and c_4

by finding the set of $\{a_i^{O_3}, a_i^{Air}\}$ coefficients that minimize the merit function M

$$M = \sum_{j=1}^{J} \left(\frac{T_m - T_e}{\sigma(h_0(j))} \right)^2 \quad (10)$$

where $T_m = T_m(h_0(j); a_0^{O_3}, ...a_{N_{O_3}}^{O_3}, a_0^{Air}, ...a_{N_{Air}}^{Air})$ and $T_e = T_e(h_0(j))$ respectively refer to the modelled and experimental transmittances at $J = 81$ tangent altitudes (1 km steps from 30 km to 110 km) during the occultation. The experimental errors $\sigma(h_0(j))$ were estimated by taking into account digitization and offset determination errors. The minimization of M was performed by using a standard Levenberg-Marquardt algorithm applied to 23 unknowns (N_{O_3}=17, N_{Air}=6).

At the minimum, the error on the solution was estimated by means of the Jacobian matrix of M [*Press et al.*, 1992] and quadratically added to errors coming from wavelength and Sun angular size discretization, temperature dependence of the ozone cross section, orbital elements and error estimation of the filter function spectral parameters. We also checked that the solution quality was insensitive to a supplementary optimization of the empirical filter function with respect to the solution profiles. This proves, a posteriori, that the use of climatological profiles was accurate enough for computing the filter function before the vertical inversion.

3. Results and discussion

From the initial 7000 occultations, we rejected all events where the satellite attitude did not have the required stability. Further, we stopped the Levenberg-Marquard optimization after 25 iterations in case of slow convergence and considered the event as not valid. Also, outlier solutions with respect to a 2-sigma level for any altitude were considered as unrealistic and rejected. Finally, a data set of 2530 profiles was obtained.

Figure 4 shows the averaged ozone profiles retrieved from the ORA experiment and the corresponding MLS (composite of 183 GHz and 205 GHz data), HALOE and SME profiles averaged during the period Aug 1992-Apr 1993 between 40S and 40N. Although the instrumental sensitivity limit is reached at about 110 km through the digitization error, we expected the averaged error to be reduced by a factor of $\sqrt{2530} \simeq 50$.

In order to check the consistency of the ORA retrieval, we compared profiles down to 30 km although it was not expected to obtain a better accuracy with our instrument. At 30 km, an ozone deficit of about 25 % for the ORA profile can be attributed to the effect of neglecting refraction. Between 40 and 60 km, ORA seems to exhibit an excedent of about 10-20% compatible however with the estimated error bar. This bias is attributed to the imperfect knowledge of the filter spectral properties and the temperature sensitivity of the ozone cross section in the Huggins bands.

From 60 to 90 km, considerable differences can be observed between the three instruments at the level of the mesospheric ozone minimum around 75-78 km. The HALOE profile reaches a more pronounced minimum while MLS seems to show signs of exaggerated inclusion of a priori information above 85 km. We have also included SME data [*Keating et al.*, 1996] up to about 87 km and these values lie closer to the ORA data at the ozone minimum.

The presence of the ozone maximum around 90 km is quite well understood[*Allen et al.*, 1984; *Fichtelmann and Sonnemann*, 1989; *Sonnemann et al.*, 1998]. It results from a maximal rate of ozone production reactions:

$$O + O_2 + M \rightarrow O_3 + M \quad (11)$$

due to the opposing gradients of increasing atomic oxygen and decreasing air density when altitude increases. The augmentation in atomic oxygen is itself strongly regulated by a loss reaction with OH and hence by the H_2O concentration.

The diurnal mesospheric ozone variation is very important. Atomic oxygen is converted into a large ozone excess after sunset which is strongly depleted at sunrise by photodissociation. During the day, a slow recovery of ozone occurs due to atomic oxygen production subsequent to O_2 photodissociation. This is the reason for observing a larger mesospheric ozone volume mixing ratio at sunset than at sunrise for a solar occultation experiment. Actually, the photochemical system of the mesosphere represents a para-

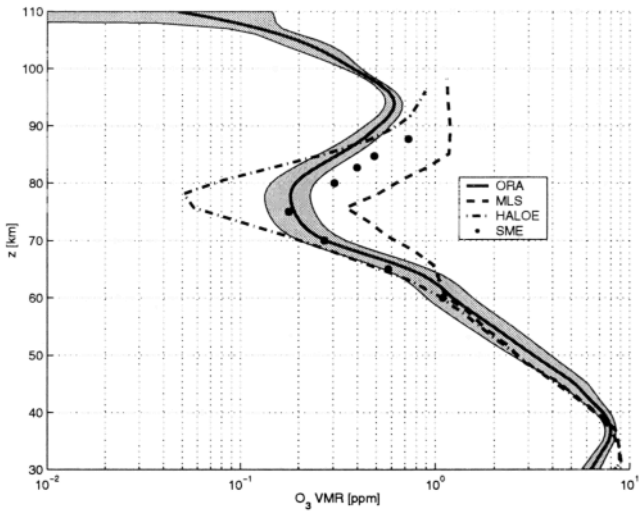

Figure 4. Intercomparison of ozone volume mixing ratio profiles obtained by the SME, MLS, HALOE and ORA instruments

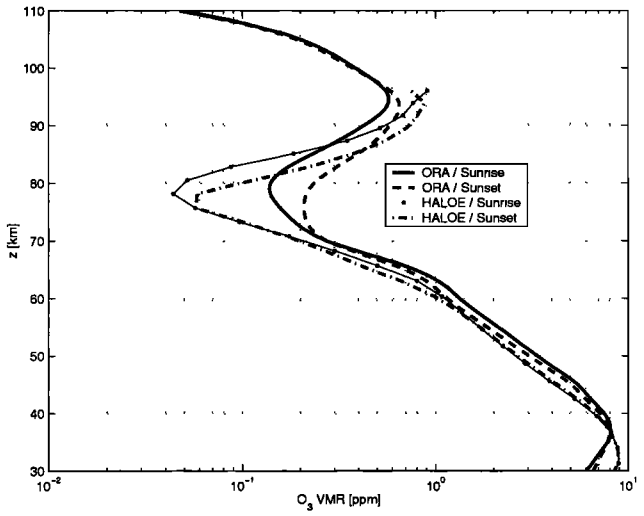

Figure 5. Intercomparison of sunrise/sunset ozone volume mixing ratio profiles for HALOE and ORA

metrically driven photochemical oscillator excited by the diurnal solar radiation leading to a resonance regime in the mesosphere [*Sonnemann and Fichtelmann*, 1997]. In Fig. 5, comparing sunrise and sunset events shows a large diurnal variation effect between 70 and 95 km for ORA and HALOE. Both instruments have a maximal variation around 83 km with a variation factor of about 1.8 for ORA and 2.5 for HALOE. It must be noticed that the retrieval algorithms (onion peeling for HALOE and the method described above for ORA) assume a radial atmosphere with no horizontal nor temporal variations of number densities. This could lead to a smoothing effect in the ORA profiles because the angular integration spans different tangent altitudes associated with different photochemical evolutions of the ozone number density along the line of sight.

Below 70 km, there is an inversion in the sunset-sunrise ratio for both instruments. This slight diurnal effect has been discussed by [*Brühl et al.*, 1996] although no definitive explanation seems to prevail.

To our knowledge, there do not exist other measurements (with extended spatial and temporal coverage) of ozone profiles above 92 km to be compared with ORA values, except for those of [*Riegler et al.*, 1977] which seem to suffer from a possible bias in this altitude range (they report a very large volume mixing ratio of more than 10 ppm at 100 km that could only be explained by critical atomic oxygen and atomic oxygen concentrations).

We conclude that the ORA UV radiometric channel has produced valuable ozone volume mixing ratio profiles in the upper atmosphere, despite a serious handicap due to its non-monochromaticity. In particular, the retrieved profiles agree satisfactorily with results of HALOE, MLS and SME up to the mesopause. Above this altitude, ORA probably supplies the first large dataset of ozone profiles in the lower thermosphere.

In future work, we will investigate the latitudinal and seasonal ozone variations. Some effort will also be devoted to the error budget estimation for the retrieval of an inhomogeneously distributed constituent in a solar occultation experiment. This could require the use of a specific photochemical model.

Acknowledgments. Two of us (F. V. and C. B.) were funded under a Prodex contract granted by the SSTC-DWTC service of the Belgian Government. This work was also supported by the 'Fonds National de la Recherche Scientifique' under grant 1.5.155.98.

References

Allen, C. W. *Astrophysical Quantities, third edition.* The Athlone Press, London and Dover, New Hampshire, 1985.

Allen, M., J. I. Lunine and Y. L. Yung. The Vertical Distribution of Ozone in the Mesosphere and Lower Thermosphere. *Journal of Geophysical Research, 89*, 4841–4872, 1984.

Brühl, C., S. R. Drayson, J. M. R. III, P. J. Crutzen, J. M. McInerney, P. N. Purcell, H. Claude, H. Gernandt, T. J. McGee, I. S. McDermid and M. R. Gunson. Halogen Occultation Experiment Ozone Channel Validation. *Journal of Geophysical Research, 101*, 10217–10240, 1996.

Burrows, J. P., A. Richter, A. Dehn, B. Deters and S. Himmelmann. Temperature-dependent cross sections of O3 in the 231-794 nm range recorded with GOME. *Journal of Quantitative Spectroscopy and Radiative Transfer, 61*, 509–517, 1999.

Fichtelmann, B. and G. Sonnemann. On the Variation of Ozone in the Upper Mesosphere and Lower Thermosphere: A Comparison Between Theory and Observation. *Zeitschrift fur Meteorologie, 39*, 297–308, 1989.

Fussen, D., E. Arijs, D. Nevejans, F. V. Hellemont, C. Brogniez and J. Lenoble. Validation of the ora spatial inversion algorithm with respect to the stratospheric aerosol and gas experiment II data. *Applied Optics, 37*, 3121–3127, 1998.

Fussen, D., E. Arijs, D. Nevejans and F. Leclere. Tomography of the Earth's Atmosphere by the Space-Borne ORA Radiometer: Spatial Inversion Algorithm. *Journal of Geophysical Research, 102*, 4357–4365, 1997.

Keating, G. M., L. S. Chiou and N. C. Hsu. Improved Ozone Reference Models for the COSPAR International Reference Atmosphere. *Advances in Space Resarch, 18*, (9/10)11–(9/10)58, 1996.

Kurucz, R., I. Furenlid, J. Brault and L. Testerman. *National Solar Observatory No1.* Harvard University, 1984.

National Oceanic and Atmospheric Organization. U. S. Standard Atmosphere. Technical report, National Aeronautics and Space Administration, United States Air Force, Washington DC, 1976.

Press, W. H., S. A. Teukolsky, W. T. Vetterling and B. P. Flannery. *Numerical Recipes in FORTRAN, Second Edition.* Cambridge University Press, Cambridge, 1992.

Riegler, G. R., S. K. Atreya, T. M. Donahue, S. C. Liu, B. Wasser and J. F. Drake. UV Stellar Occultation Measurements of Nighttime Equatorial Ozone. *Geophysical Research Letters, 4*, 145–148, 1977.

Sonnemann, G. and B. Fichtelmann. Subharmonics, cascades of period doubling, and chaotic behavior of photochemistry of the mesopause region. *Journal of Geophysical Research, 102*, 1193–1203, 1997.

Sonnemann, G., C. Kremp, A. Ebel and U. Berger. A Three-Dimensional Dynamic Model of the Minor Constituents of the Mesosphere. *Atmospheric Environment, 18*, 3157–3172, 1998.

D. Fussen, F. Vanhellemont, C. Bingen, and S. Chabrillat, Institut d'Aéronomie Spatiale de Belgique, 3, avenue Circulaire, B-1180, Brussels, BELGIUM (e-mail: Didier.Fussen@oma.be)

(Received March 3, 2000; revised June 1, 2000;
accepted August 25, 2000.)